

## Article

# Microstructure and Performance of Ni/TiN Coatings Deposited by Laser Melting Deposition on 40Cr Substrates

Yan Wang \* and Wang Gao

School of Mechanical Science and Engineering, Northeast Petroleum University, Daqing 163318, China; wanggao1234@126.com

\* Correspondence: wangyan202020@nepu.edu.cn; Tel./Fax: +86-459-650-3337

**Abstract:** The current study reports the successful preparation of Ni/TiN coatings via laser melting deposition (LMD) for repairing the shaft of an electric submersible pump (ESP). The surface morphology, microstructure, phase composition, microhardness, shear strength, and wear resistance were investigated using a scanning electron microscope (SEM), X-ray diffractometer (XRD), microhardness meter, shear strength test machine, and friction and wear tester. Among the three coatings, the Ni/TiN coating deposited at 1.5 kW processed fine grains with an evenly dispersed and compact structure. The Ni/TiN coating revealed a face-centered cubic (f c c) lattice that exhibited diverse orientations due to the laser powers. The Ni/TiN coating deposited at 1 kW had the lowest average microhardness of 768 HV, while the Ni/TiN coating deposited at 1.5 kW had the highest average hardness of 843 HV. The shear displacements of the Ni/TiN coatings obtained at 1, 1.5, and 2 kW were 0.68, 0.54, and 0.61 mm, respectively. The Ni/TiN coating deposited at 1.5 kW had the lowest friction coefficient among all coatings, with an average value of only 0.44. Additionally, the Ni/TiN coating deposited at 1.5 kW exhibited the highest wear resistance. The presence of Ni, Ti, N, Cr, and Fe elements on the surface of the shaft of the ESP, indicated that the LMD technology had successfully repaired the shaft.



**Citation:** Wang, Y.; Gao, W. Microstructure and Performance of Ni/TiN Coatings Deposited by Laser Melting Deposition on 40Cr Substrates. *Coatings* **2022**, *12*, 367. <https://doi.org/10.3390/coatings12030367>

Academic Editor: You Seung Rim

Received: 2 February 2022

Accepted: 7 March 2022

Published: 10 March 2022

**Publisher's Note:** MDPI stays neutral with regard to jurisdictional claims in published maps and institutional affiliations.



**Copyright:** © 2022 by the authors. Licensee MDPI, Basel, Switzerland. This article is an open access article distributed under the terms and conditions of the Creative Commons Attribution (CC BY) license (<https://creativecommons.org/licenses/by/4.0/>).

**Keywords:** laser melting deposition; Ni/TiN coating; microstructure; shear strength; wear resistance

## 1. Introduction

The 40Cr steel (GB/T17107-2018) is generally used for manufacturing the shaft of an electric submersible pump (ESP) [1]. However, during a long-term operation, the shaft of the ESP is prone to wear and corrosion due to sand particles, acid liquid, poor lubrication, and other factors [2–4]. Some repair methods, such as electrospark deposition, brushing electrodeposition, plasma arc deposition, and laser melting deposition can be used to refabricate the shaft when it is worn or corroded [5–8]. Among all deposition techniques, laser melting deposition (LMD) has the advantages of high coating quality, high flexibility, rapid processing rate, and high binding strength, allowing the production of metal-ceramic composite coatings with outstanding physical and chemical properties. Xia et al. [9] demonstrated the fabrication of nickel-based WC coatings by the LMD technique. The results indicated that WC particles might be used to enhance the coating's corrosion resistance. The LMD approach was successfully used to fabricate reduced activation steels by An et al. [10]. They found that the grain sizes in the upper layers were larger than those in the substrate. Salman et al. [11] investigated the effect of heat treatment on the microstructure and composition of 316L stainless steel. They found that laser power could affect the microstructure, phases, and composition of the steel.

Titanium nitride (TiN) is a common metal nitride with high elastic modulus and hardness that is typically used to improve the properties of metals or alloys, such as Ni/TiN coatings, Al<sub>2</sub>O<sub>3</sub>/TiN coatings, Al-Cu/TiN coatings, and so on [12–15]. Ni/TiN coatings have recently gained increasing scientific attention due to their high hardness,

excellent wear and corrosion resistance, and excellent oxidation and high-temperature mechanical properties. Wu et al. [16] have proved the synthesis of Ni/TiN coatings prepared through electrodeposition. Their findings indicated that the Ni/TiN coatings possessed excellent wear resistance. Peng et al. [17] studied the corrosion rates of Ni/TiN coatings produced using magnetic electrodeposition. Wang et al. [18] discussed the fabrication of TiN/Ni coatings using a plasma transferred arc scanning process. The results revealed that appropriate parameters could improve the corrosion resistance of TiN/Ni coatings.

Although many studies on the fabrication of TiN/Ni coatings have been published [19–21], there are relatively few reports on the synthesis of Ni/TiN coatings by the LMD technique. Furthermore, few studies on the microstructure and performance of LMD-deposited Ni/TiN coatings have been published to date. In this study, the Ni/TiN coatings were synthesized using the LMD method, and their surface morphology, microstructure, phase composition, microhardness, shear strength, and wear resistance were analyzed using a scanning electron microscope (SEM), an X-ray diffractometer (XRD), a microhardness meter, a shear strength test machine, and a friction and wear tester.

## 2. Experimental Procedure

### 2.1. Preparation

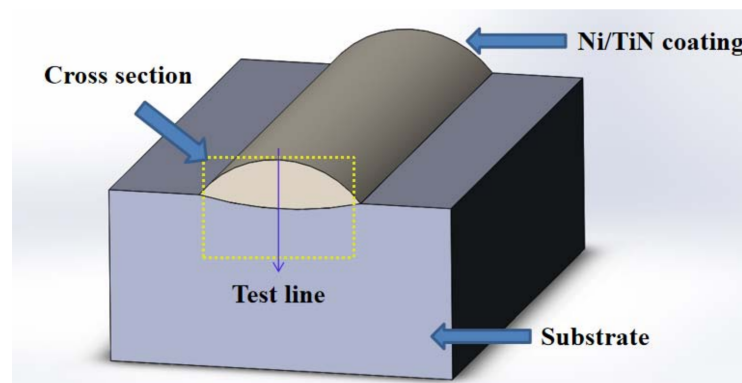
The Ni powders and TiN microparticles were purchased from Shanghai Tianshun Technology Co., Ltd. (Shanghai, China) The average sizes of TiN microparticles and Ni powders were approximately 10 and 20  $\mu\text{m}$ , respectively. Prior to LMD, Ni powders and TiN microparticles were mixed in 8:2 ratios and dried for 60 min at 65  $^{\circ}\text{C}$  in a DX-100 type drying box. The 40Cr substrate (80 mm  $\times$  30 mm  $\times$  10 mm) was immersed in acetone and then washed with an ultrasonic cleaner of UXL-200 type. The ultrasonic power and time were kept at 200 W and 30 min, respectively. The Ni/TiN coatings were prepared on the 40Cr surface using a LM-200WA Laser Melting Machine (Changchun Laser Technology Co., Ltd., Changchun, China), as shown in Figure 1. The parameters for producing Ni/TiN coatings are listed as follows: the powder delivery rate 0.6 m/s, the Argon flow rate 1.5 m/s, and the laser scanning rate 4 mm/s. According to the parameters of the LM-200WA laser melting machine and the relevant literatures [22,23], the laser powers were set at 1, 1.5, and 2 kW, respectively. The thickness of the coating was kept at 2 mm to reduce the effect of thickness on the performance of Ni/TiN coatings by controlling the amount of Ni powders and TiN microparticles. In addition, twelve Ni/TiN samples were obtained by using laser powers of 1, 1.5, and 2 kW.



Figure 1. Physical image of the laser melting machine.

## 2.2. Measurement

The surface morphology and crystal phase structure of Ni/TiN coatings were studied using a scanning electron microscope (SEM, S3400, Hitachi High-Tech Corporation, Tokyo, Japan) and X-ray diffraction (XRD, D5000, Siemens, Munich, Germany). The test parameters were as follows: Cu K $\alpha$  radiation, scan step of 0.05°/s, the scan range of 20–90°, tube voltage of 40 kV, and tube current of 100 mA. Before the SEM analysis, the surfaces of Ni/TiN coatings were washed with acetone and deionized water. The microhardness of Ni/TiN coatings was measured using a DHS-1000 microhardness tester at room temperature. The coating's microhardness was determined along the test line, as illustrated in Figure 2. The load was 1.96 N and the time was 15 s, respectively. The Ni/TiN coatings were polished with 400, 800, 100, and 1200 grit emery papers sequentially before the microhardness test.



**Figure 2.** Sampling position for testing the microhardness of Ni/TiN coating.

Prior to the shear strength test, the samples were cut into 50 mm  $\times$  20 mm  $\times$  1 mm size using a DK773-A type wire electric-discharge machine (Taizhou Zhongrui Machine Tool Co., Ltd., Taizhou, China). The shear head had a diameter of 2 mm and a loading rate of 0.5 mm/min. The wear resistance of the Ni/TiN coatings was evaluated using a UMT-3G friction wear tester. The grinding ball had a diameter of 3 mm and was made of GCr15 steel (60 HRC), with a rotation rate and time of 150 r/min and 30 min, respectively. After the wear tests, the SEM was used for analyzing the worn morphologies of the coatings.

## 3. Results and Discussion

### 3.1. Surface Morphology

The surface morphologies of Ni/TiN coatings produced at various laser powers are shown in Figure 3. The Ni/TiN coating obtained at 1 kW had a coarse morphology with large TiN particles. Among the three coatings, the Ni/TiN coating deposited at 1.5 kW showed fine grains that were evenly dispersed and had a compact structure. However, the Ni/TiN coating deposited at 2 kW exhibited a structure with larger grains than that of the Ni/TiN coating deposited at 1.5 kW.

The phenomenon can be explained by the fact that TiN particles have a melting point of 3290 °C, whereas nickel has a melting point of 1455 °C [24]. Nickel powders were completely melted when the laser power was 1 kW. Numerous TiN particles, however, could not be melted, and so the unmelted TiN particles with a large size were wrapped into the coating by the melted nickel crystals. As a result, the Ni/TiN coating produced at 1 kW exhibited a coarse morphology with large TiN particles. When the laser power was set to 1.5 kW, the nickel powders and TiN particles were thoroughly melted, resulting in fine grains that were evenly dispersed and compact in the coating. However, if excessive laser power (i.e., 2 kW) was used, the large amounts of thermal energy generated by the laser beam could cause Ni grains to melt and grow rapidly. Meanwhile, TiN particles reconnected as a result of the high thermal energy [25]. These findings are in good agreement with those reported by Wang et al. [26].

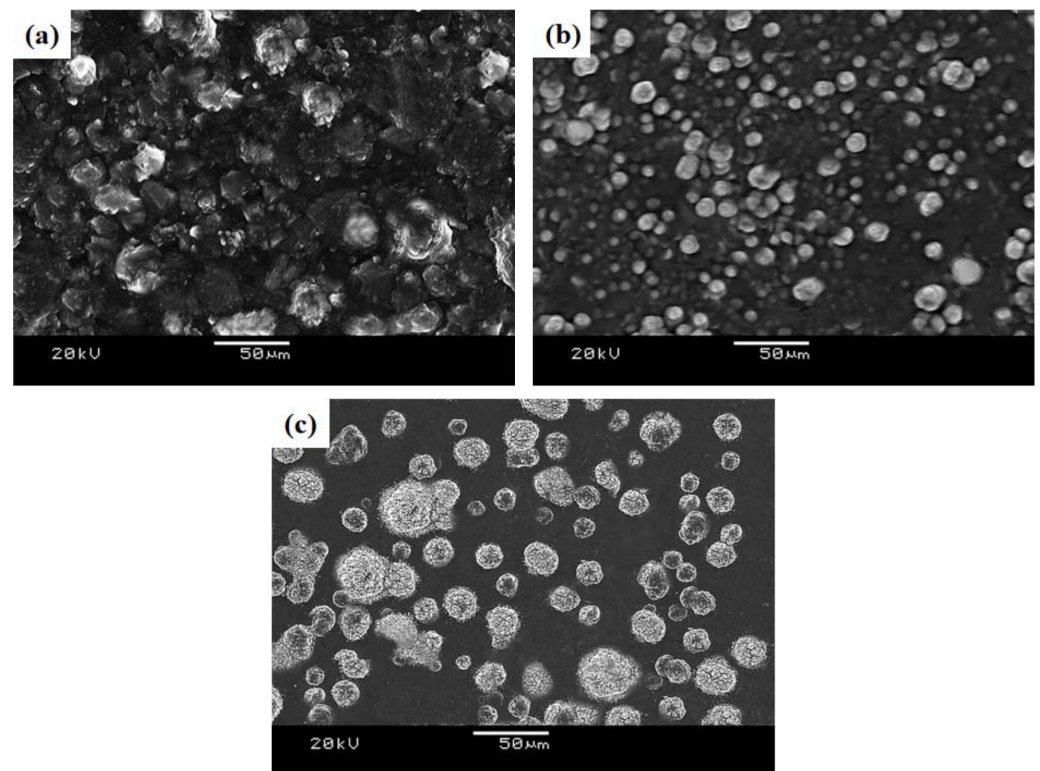


**Figure 3.** SEM images of Ni/TiN coatings produced at various laser powers: (a) 1 kW, (b) 1.5 kW, (c) 2 kW.

### 3.2. XRD Analysis

The XRD patterns of the Ni/TiN coatings produced with various laser powers are shown in Figure 4. The figure shows that the Ni/TiN coating displayed a face-centered cubic (f c c) lattice with a variety of orientations due to the laser powers. The results are similar to those reported by Chen et al. [27]. Furthermore, Ni, TiNi, Ti<sub>2</sub>Ni, and TiN phases were present in the Ni/TiN coating. This phenomenon can be explained as follows:

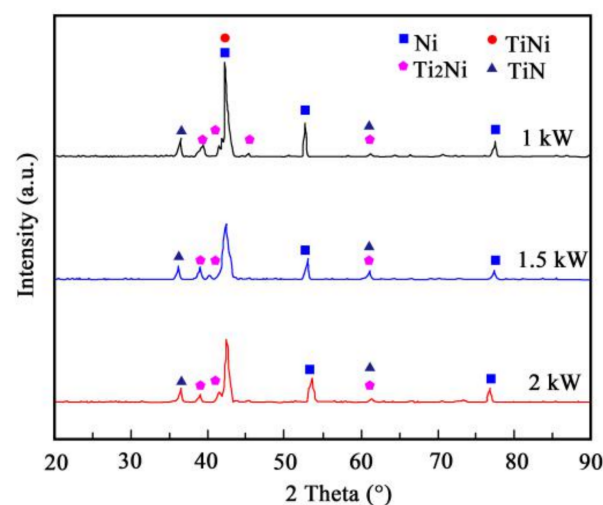


**Figure 4.** XRD images of Ni/TiN coatings produced at various laser powers.

Additionally, among all Ni/TiN coatings, the 1.5 kW coating had the lowest and widest diffraction peaks, indicating that fine grains and a compact microstructure were formed in this coating. The results are consistent with those obtained through SEM analysis.

### 3.3. Microhardness Test

The microhardness curves of the Ni/TiN coatings prepared using different laser powers are displayed in Figure 5. The laser power had a significant influence on the microhardness of the Ni/TiN coatings but had less influence on the microhardness of the substrate. The average microhardness of the substrate was 385 HV, which was significantly less than the microhardness of the Ni/TiN coatings. Additionally, the Ni/TiN coating deposited at 1 kW had an average microhardness of 768 HV, the lowest of the three coatings, but the Ni/TiN coating deposited at 1.5 kW had a maximum average microhardness of 843 HV. However, the Ni/TiN coating produced an average hardness of 808 HV when it was fabricated at 2 kW.

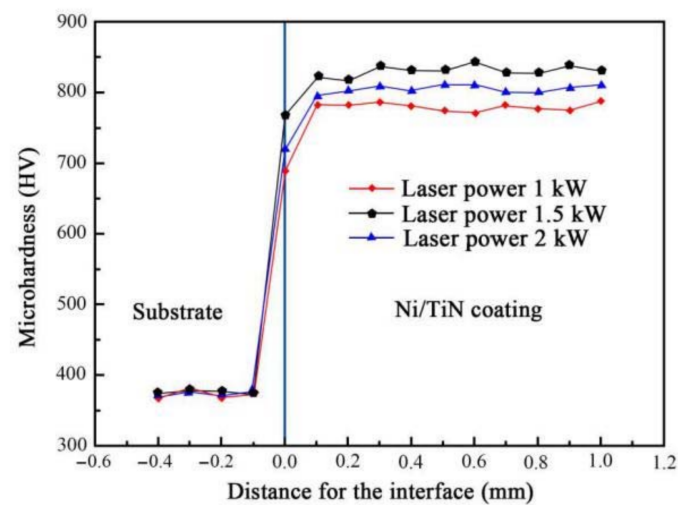
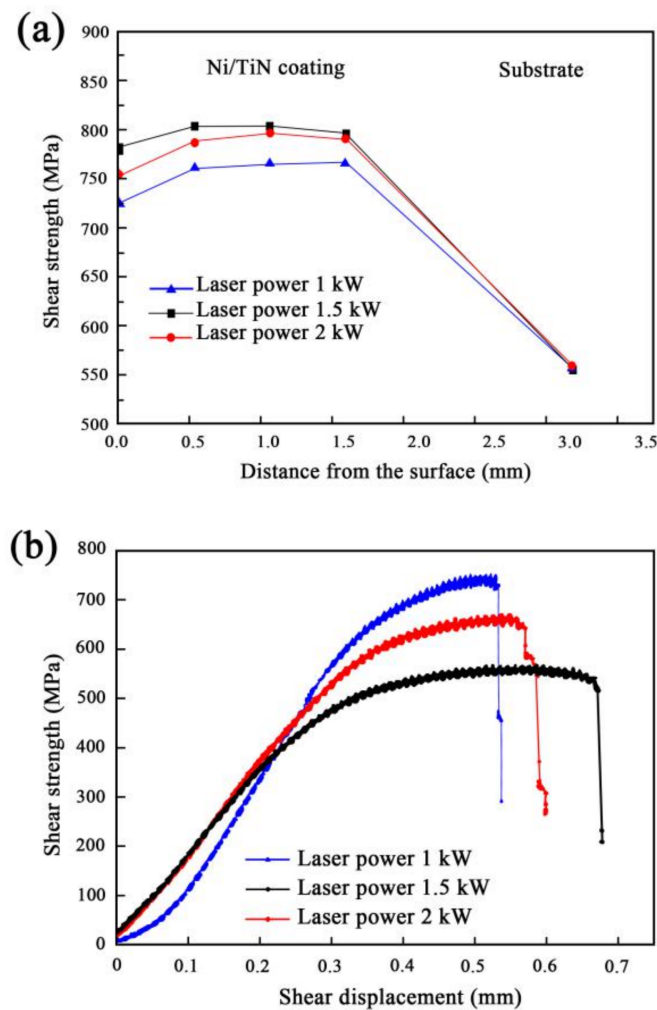


**Figure 5.** Microhardnesses of Ni/TiN coatings produced at various laser powers.

The refined grains had a significant reinforcing effect on the melting layer during the LMD process [28]. Additionally, the hard TiNi, Ti<sub>2</sub>Ni, and TiN particles scattered in Ni/TiN coatings aided in dispersion reinforcement. Thus, the three Ni/TiN coatings had significantly higher microhardness than the matrix. In particular, the coating obtained at 1.5 kW had the smallest internal microstructure and the greatest fine crystal reinforcement effect of the others. As a result, the coating had the highest microhardness.

### 3.4. Shear Strength Test

Figure 6 presents the shear strength and displacement of Ni/TiN coatings produced at different laser powers. The shear strengths of Ni/TiN coatings were found to be significantly higher than those of the substrate, as shown in Figure 6a. Due to the coating's fine and compact structure having the maximum microhardness, the Ni/TiN coating deposited at 1.5 kW had an average shear strength of 802 MPa, which was much greater than the shear strengths of the other coatings [29]. The shear strength of the substrate was only 557 MPa, which was greater than the shear strength of 40Cr (400 MPa). This was due to the laser heating the 40Cr substrate, which increased the shear strength.



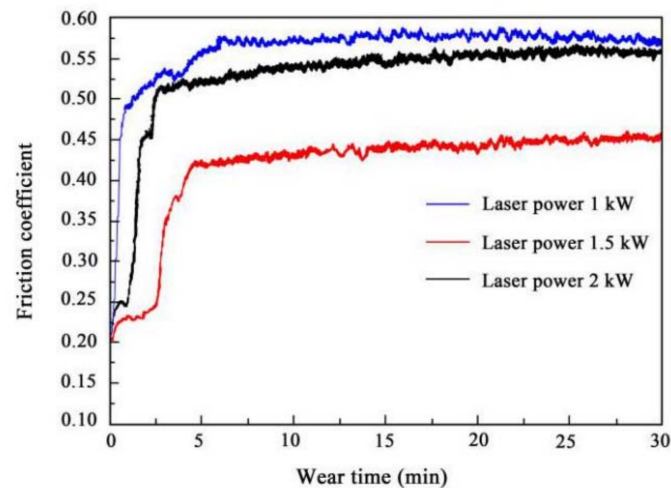
**Figure 6.** Shear strength curves (a) and shear displacement curves (b) of Ni/TiN coatings produced at various laser powers.

Figure 6b reveals the shear displacements of Ni/TiN coatings deposited at various laser powers. The shear displacements of the Ni/TiN coatings obtained at 1, 1.5, and 2 kW were 0.68, 0.54, and 0.61 mm, respectively. Due to the high shear strength of the Ni/TiN coating produced at 1.5 kW, it displayed the least displacement of all Ni/TiN coatings.

### 3.5. Wear Resistance Measurement

Figure 7 illustrates the effect of laser power on friction coefficients of Ni/TiN coatings deposited by the LMD method. During wear experiments, all three Ni/TiN coatings were subjected to both initial and stable wear stages. The friction coefficients of three Ni/TiN coatings rapidly increased as the wear time increased from 0 to 5 min. Because the uneven surfaces of the Ni/TiN coatings caused the grinding ball to move violently up and down, the friction coefficient increased. Five minutes later, the surfaces of Ni/TiN coatings were flattened, and then, the friction coefficients of all three Ni/TiN coatings changed smoothly.

Additionally, the Ni/TiN coating produced at 1.5 kW had the lowest friction coefficient among all coatings, with an average value of only 0.44. The friction coefficient of Ni/TiN coating deposited at 1 kW, on the other hand, had the highest value of 0.58. While the average friction coefficient of the Ni/TiN coating obtained at 2 kW was 0.54. The reason for this was that Ni/TiN coatings with fine tissue and high microhardness could be deposited at appropriate laser power (i.e., 1.5 kW), resulting in the lowest friction coefficient.



**Figure 7.** Friction coefficients of Ni/TiN coatings produced at various laser powers.

The effect of laser power on the worn morphologies of Ni/TiN coatings deposited using the LMD technique is shown in Figure 8. Many deep grooves appeared on the surface of the Ni/TiN coatings deposited at 1 kW. Meanwhile, some large abrasive chips appeared on the surface of the coating (Figure 8a). However, there were only a few shallow scratches on the surface of Ni/TiN coatings deposited at 1.5 kW (Figure 8b). When the laser power was increased to 2 kW, the grooves on the surface of the Ni/TiN coatings grew deeper, and the abrasive chips reappeared (Figure 8c). The Ni/TiN coating deposited at 1.5 kW had the best wear resistance among the three coatings tested. The reason for this was that using an appropriate laser power, Ni/TiN coatings with fine microstructure and high microhardness could be deposited. As a result, the coating was able to resist external forces more effectively and significantly improved its wear resistance. These experimental results are consistent with that reported by Li et al. [30].

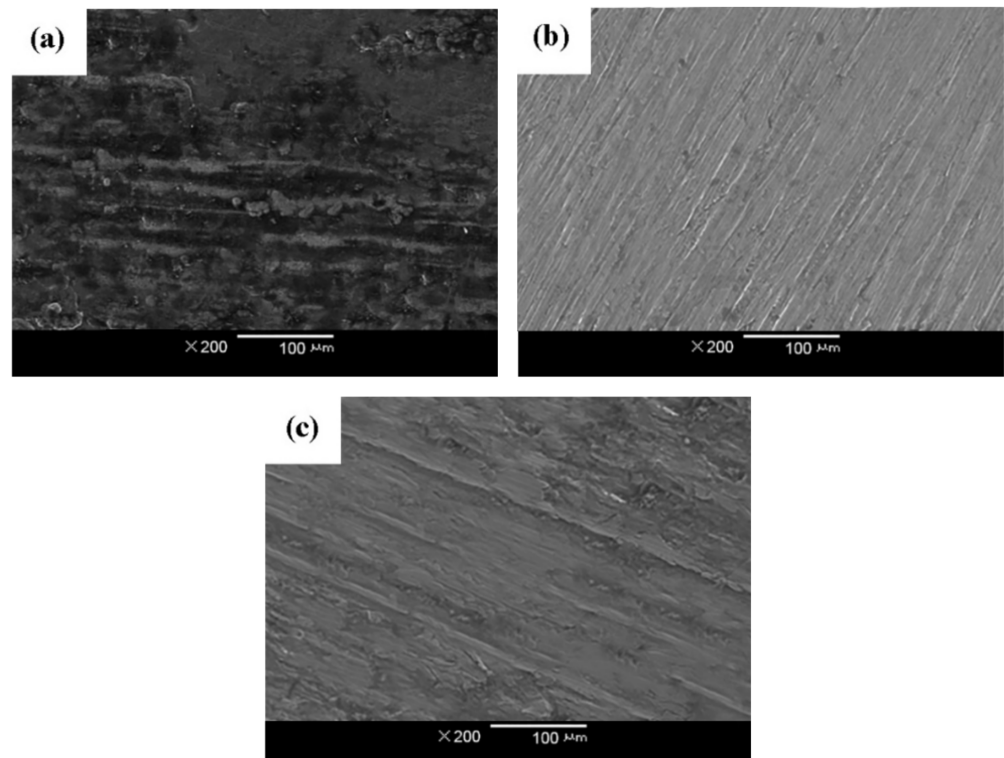


**Figure 8.** Worn images of Ni/TiN coatings produced at various laser powers: (a) 1 kW, (b) 1.5 kW, (c) 2 kW.

In summary, an outstanding Ni/TiN coating could be manufactured by using the following LMD parameters: the powder delivery rate of 0.6 m/s, the Argon flow rate of 1.5 m/s, the laser scanning rate of 4 mm/s, and the laser power of 1.5 kW. In addition, the shaft of the ESP was successfully repaired by using the above-mentioned parameters, as shown in Figure 9. The Ni/TiN coating was found to be tightly combined with the shaft after grinding. Ni, Ti, N, Cr, and Fe elements appeared on the surface of the shaft of the ESP, indicating that the LMD technology had successfully repaired the shaft of the ESP.

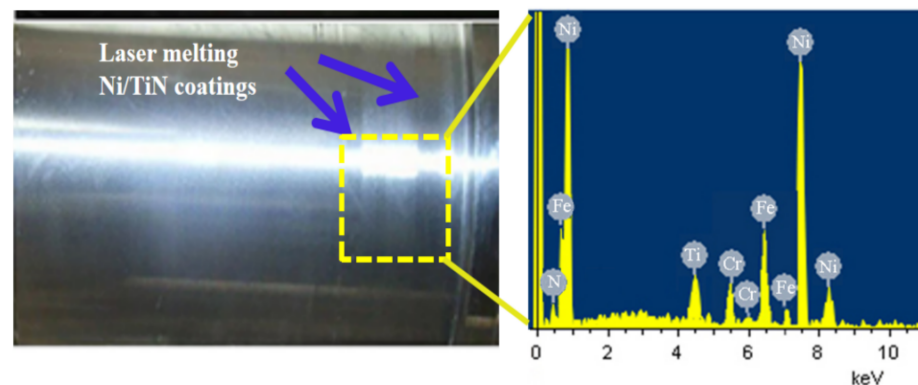


**Figure 9.** Image of the shaft of the ESP after repair by using LMD technique.

#### 4. Conclusions

In this study, Ni/TiN coatings were fabricated by using laser melting deposition, and some conclusions were listed as follows:

- (1) The Ni/TiN coating deposited at 1 kW exhibited a coarse morphology with large TiN particles. Among the three coatings, the Ni/TiN coating deposited at 1.5 kW processed fine grains that were evenly dispersed and had a compact microstructure. The Ni/TiN coating displayed a face-centered cubic (fcc) lattice, which exhibited a variety of orientations due to the laser powers.
- (2) The Ni/TiN coating deposited at 1 kW had an average microhardness of 768 HV, the lowest of the three coatings, whereas the Ni/TiN coating deposited at 1.5 kW had a maximum average microhardness of 843 HV. However, the Ni/TiN coating processed an average hardness of 808 HV when prefabricated at 2 kW.
- (3) The Ni/TiN coating deposited at 1.5 kW processed an average shear strength of 802 MPa, which was significantly higher than the shear strengths of the other coatings. The shear displacements of the Ni/TiN coatings obtained at 1, 1.5, and 2 kW were 0.68, 0.54, and 0.61 mm, respectively. The Ni/TiN coating produced at 1.5 kW had the lowest friction coefficient of all coatings, with an average value of only 0.44. Additionally, the Ni/TiN coating deposited at 1.5 kW had the best wear resistance of the three coatings.
- (4) The Ni/TiN coating was tightly combined with the shaft after grinding. Ni, Ti, N, Cr, and Fe elements appeared on the surface of the shaft of the ESP, indicating that the LMD technology had successfully repaired the shaft of the ESP.

**Author Contributions:** Study design and collection of data, Figures, study design, writing—original draft preparation, Y.W.; data analysis, data interpretation, W.G. All authors have read and agreed to the published version of the manuscript.

**Funding:** This work has been supported by the US-China Clean Energy Research Centre Joint Work Plan for Research Projects on Water Energy Technologies (Granted No. 2018YFE019600) and the Guided Innovation Foundation Project of Northeast Petroleum University (Granted No. 2019YDL-15).

**Institutional Review Board Statement:** Not applicable.

**Informed Consent Statement:** Not applicable.

**Data Availability Statement:** Data are contained within the article.

**Conflicts of Interest:** The authors declare that they have no known competing financial interest or personal relationships that could have appeared to influence the work reported in this paper.

## References

1. Yan, S.; Luo, X.; Sun, S.; Zhang, L.; Chen, S.; Feng, J. Influence of inlet gas volume fraction on energy conversion characteristics of multistage electric submersible pump. *J. Petrol. Sci. Eng.* **2021**, *207*, 109164. [\[CrossRef\]](#)
2. Reges, G.; Fontana, M.; Ribeiro, M.; Silva, T.; Schnitman, L. Electric submersible pump vibration analysis under several operational conditions for vibration fault differential diagnosis. *Ocean Eng.* **2020**, *219*, 108249. [\[CrossRef\]](#)
3. Martins, J.R.; Ribeiro, D.D.C.; Assis, F.D.; Pereira, R.; Romero, O.J. Heat dissipation of the electrical submersible pump (ESP) installed in a subsea skid. *Oil Gas Sci. Technol.* **2020**, *75*, 13. [\[CrossRef\]](#)
4. Liu, Z.; Sun, B.; Wang, Z.; Lou, W.; Zhang, J. Modeling of multiphase flow in marine gas hydrate production system and its application to control the production pressure difference. *J. Nat. Gas Sci. Eng.* **2020**, *85*, 103687. [\[CrossRef\]](#)
5. Burkov, A.; Kulik, M.; Krutikova, V. Electrospark deposition of tungsten carbide powder on titanium alloy Ti<sub>6</sub>Al<sub>4</sub>V. *Lett. Mater.* **2021**, *11*, 175–180. [\[CrossRef\]](#)
6. Choi, K.H.; Han, S.K.; Lee, T.H. Electrode fabrication for proton exchange membrane fuel cells by pulse electrodeposition. *J. Power Sources* **1998**, *75*, 230–235. [\[CrossRef\]](#)
7. Krysinina, O.V.; Yu, F.I.; Koval, N.N.; Prokopenko, N.A.; Shugurov, V.V.; Petrikova, E.A.; Tolkachev, O.S. Composition, structure and properties of Mo-N coatings formed by the method of vacuum-arc plasma-assisted deposition. *Surf. Coat. Technol.* **2021**, *416*, 127153. [\[CrossRef\]](#)
8. Wang, L.; Gao, M.; Zhang, C.; Zeng, X. Effect of beam oscillating pattern on weld characterization of laser welding of AA6061-T6 aluminum alloy. *Mater. Des.* **2016**, *108*, 707–717. [\[CrossRef\]](#)
9. Xia, Y.; Chen, H.; Liang, X.; Lei, J. Circular oscillating laser melting deposition of nickel-based superalloy reinforced by WC: Microstructure, wear resistance and electrochemical properties. *J. Manuf. Process.* **2021**, *68*, 1694–1704. [\[CrossRef\]](#)
10. An, Q.; Xia, Z.X.; Zhang, C.; Yang, Z.G.; Chen, H. Effect of thermal cycles on microstructure of reduced activation steel fabricated using laser melting deposition. *J. Iron Steel Res. Int.* **2021**, *28*, 316–326. [\[CrossRef\]](#)
11. Salman, O.O.; Gammmer, C.; Chaubey, A.K.; Eckert, J.; Scudino, S. Effect of heat treatment on microstructure and mechanical properties of 316L steel synthesized by selective laser melting. *Mater. Sci. Eng.* **2019**, *748*, 205–212. [\[CrossRef\]](#)
12. Xia, F.; Li, C.; Ma, C.; Li, Q.; Xing, H. Effect of pulse current density on microstructure and wear property of Ni-TiN nanocoatings deposited via pulse electrodeposition. *Appl. Surf. Sci.* **2021**, *538*, 148139. [\[CrossRef\]](#)
13. Li, W.Y.; Zhang, G.; Liao, H.L.; Coddet, C. Characterizations of cold sprayed TiN particle reinforced Al2319 composite coating. *J. Mater. Process. Technol.* **2008**, *202*, 508–513. [\[CrossRef\]](#)
14. Chi, F.; Schmerling, M.; Eliezer, Z.; Marcus, H.L.; Fine, M.E. Preparation of Cu-TiN alloy by external nitridation in combination with mechanical alloying. *Mater. Sci. Eng. A* **1995**, *190*, 181–186. [\[CrossRef\]](#)
15. Li, X.; Zhu, Y.; Xiao, G. Application of artificial neural networks to predict sliding wear resistance of Ni-TiN nanocomposite coatings deposited by pulse electrodeposition. *Ceram. Int.* **2014**, *40*, 11767–11772. [\[CrossRef\]](#)
16. Wu, M.; Jia, W.; Lv, P. Electrodepositing Ni-TiN nanocomposite layers with applying action of ultrasonic waves. *Procedia Eng.* **2017**, *174*, 717–723. [\[CrossRef\]](#)
17. Peng, X.S.; Li, Y.P.; Zhang, X.M.; Wang, S. Prediction on corrosion rate of Ni-TiN coatings by BP neural network. *J. Synth. Cryst.* **2016**, *45*, 2556–2560. (In Chinese)
18. Wang, W.; Qian, S.Q.; Zhou, X.Y. Microstructure and properties of TiN/Ni composite coating prepared by plasma transferred arc scanning process. *Trans. Nonferrous Met. Soc. China* **2009**, *19*, 1180–1184. [\[CrossRef\]](#)
19. Kumar, M.; Mitra, R. Effect of substrate temperature and annealing on structure, stress and properties of reactively co-sputtered Ni-TiN nanocomposite thin films. *Thin Solid Films* **2017**, *624*, 70–82. [\[CrossRef\]](#)
20. Sun, W.; Jin, S.; Yu, Y. Preparation and characterization of Ni-TiN ultrafine powder. *Powder Metall. Technol.* **2000**, *332*, 356–361.
21. Zhu, X.B.; Cai, C.; Zheng, G.Q.; Zhang, Z. Electrodeposition and corrosion behavior of nanostructured Ni-TiN composite films. *Trans. Nonferrous Met. Soc. China* **2011**, *21*, 2216–2224. [\[CrossRef\]](#)
22. He, X.Y. Cause analysis of turbine rotor's shaft neck damage and the repair. *Power Equip.* **2009**, *23*, 170–172. (In Chinese)
23. Shchurova, A.V. Modeling the turbine rotor journal restoration located on cylindrical surface of the supporting bearer. *Procedia Eng.* **2017**, *206*, 1142–1147. [\[CrossRef\]](#)
24. El-Genk, M.S.; Tournier, J.M. A review of refractory metal alloys and mechanically alloyed-oxide dispersion strengthened steels for space nuclear power systems. *J. Nucl. Mater.* **2005**, *340*, 93–112. [\[CrossRef\]](#)
25. Zhang, X.P.; Zhang, Z.K.; Cui, Z.L. Preparation and characterization of nano-TiN particles. *J. Qingdao Univ. Sci. Technol.* **2004**, *3*, 235–237.
26. Wang, R.J.; Liang, J.L.; Huang, X.Y.; Shi, H.X. Microstructure and corrosion properties of laser cladding CoCrW coating on 37Mn5 steel surface of oil and gas pipeline. *Mater. Sci. Eng. Power Metall.* **2020**, *25*, 475–479.
27. Chen, X.; Cheng, H.Y. Graphical simulation for microstructures of Ni-TiN coatings using cellular automata model. *Adv. Mater. Res.* **2014**, *912*, 154–157. [\[CrossRef\]](#)

28. Fang, H.; Wang, S.; Chen, R.; Xu, Q.; Yan, Y.; Su, Y.; Guo, J. The effects of the formation of a multi-scale reinforcing phase on the microstructure evolution and mechanical properties of a Ti<sub>2</sub>AlC/TiAl alloy. *Nanoscale* **2021**, *13*, 12565–12576. [[CrossRef](#)]
29. Nur-E-Alam, M.; Rahman, M.M.; Basher, M.K.; Vasiliev, M.; Alameh, K. Optical and chromaticity properties of metal-dielectric composite-based multilayer thin-film structures prepared by RF magnetron sputtering. *Coatings* **2020**, *10*, 251. [[CrossRef](#)]
30. Li, L.; Sun, F.; Zhang, Y.C. Effect of solution treatment on the performance of laser cladding Satellite 6 alloy coating. *Surf. Technol.* **2017**, *46*, 78–81.